

# Quantum Advantage with Seeded Squeezed Light for Absorption Measurement

Fu Li,<sup>1,2,\*</sup> Tian Li,<sup>1,3,†</sup> Marlan O. Scully,<sup>1,4,5</sup> and Girish S. Agarwal<sup>1,2,3</sup>


<sup>1</sup>*Institute for Quantum Science and Engineering, Texas A&M University, College Station, Texas 77843, USA*

<sup>2</sup>*Department of Physics and Astronomy, Texas A&M University, College Station, Texas 77843, USA*

<sup>3</sup>*Department of Biological and Agricultural Engineering, Texas A&M University, College Station, Texas 77843, USA*

<sup>4</sup>*Department of Mechanical and Aerospace Engineering, Princeton University, Princeton, New Jersey 08544, USA*

<sup>5</sup>*Quantum Optics Laboratory, Baylor Research and Innovation Collaborative, Waco, Texas 76704, USA*

 (Received 5 March 2021; revised 1 April 2021; accepted 2 April 2021; published 20 April 2021)

Absorption measurement is an exceptionally versatile tool for many applications in science and engineering. For absorption measurements using laser beams of light, the sensitivity is theoretically limited by the shot noise due to the fundamental Poisson distribution of the photon number in laser radiation. In practice, the shot-noise limit can only be achieved when all other sources of noise are eliminated. Here, we use seeded squeezed light to demonstrate that direct-absorption measurements can be performed with a sensitivity beyond the shot-noise limit. We present a practically realizable scheme, where intensity-squeezed beams are generated by a seeded four-wave mixing process in an atomic rubidium-vapor cell. More than 1.2 dB quantum advantage for the measurement sensitivity is obtained at faint absorption levels ( $\leq 10\%$ ). We also present a detailed theoretical analysis to show that the observed quantum advantage when corrected for optical loss would be equivalent to 3 dB. Our experiment demonstrates a direct sub-shot-noise measurement of absorption that requires neither homodyne or lock-in nor logic coincidence-detection schemes. It is therefore very applicable in many circumstances where sub-shot-noise-level absorption measurements are highly desirable.

DOI: [10.1103/PhysRevApplied.15.044030](https://doi.org/10.1103/PhysRevApplied.15.044030)

## I. INTRODUCTION

It has been demonstrated that one can improve the sensitivity and precision of many classical measurement techniques using various quantum states of light [1–14] (for instance, the experimental work reported in Ref. [1] is a sub-shot-noise measurement of an intensity modulation on one of the quantum-correlated twin beams and the intensity is modulated by adjusting the transmission of the beam from a liquid-crystal cell). Most prominently, sub-shot-noise detection of changes in optical phase have been demonstrated in interferometers using quantum light [15–18] and have been implemented for gravitational-wave detection [19]. Although a straightforward readily attainable approach to achieve desired performances of a classical measurement is to simply increase the photon flux of the probe light to yield a greater signal-to-noise ratio, it has been proven unfeasible whenever one faces limits on the brightness of the optical probes; for instance, in the case where samples can be altered or damaged by

the probe light [11,20]. It is therefore highly desirable to optimize measurement sensitivity with a fixed amount of input photon flux [11]. It is also important to note that for measurement schemes where the sensitivity itself varies with parameters of the measured sample, it is possible for the sensitivity to be degraded, potentially requiring either prior knowledge about the optical sample or the addition of a feedback servo loop to ensure a sub-shot-noise performance [21–23].

Since the intensity measurement of an idealized laser fluctuates with a Poisson distribution, it is therefore used to define the shot-noise limit (SNL) in optical measurements and it can only be reached in classical experiments once all other sources of noise are removed. For a direct measurement of optical transmission, the number of photons that pass through a sample is used to estimate the absorption  $\alpha$  of the sample and thus the estimation sensitivity  $\Delta\alpha$  is determined by the SNL. One of the most popular approaches that allow for a sub-SNL measurement of the absorption of an unknown sample is to use quantum-correlated beams of photons [12,13]. For practical applications, the reduction of noise between quantum-correlated beams of photons generated with spontaneous parametric down-conversion (SPDC) is widely adopted because of the

\*fuli@physics.tamu.edu

†tian.li@tamu.edu

‡These authors contributed equally to this work.

simplicity of implementation and the robustness of quantum nature against the introduction of an absorbing sample [24]. In particular, such a technique has been implemented in the context of imaging, where a charge-coupled-device (CCD) camera is usually employed to acquire sub-SNL measurements in the spatial domain by detecting correlated photons altogether in the same image captured by the camera [6,8,25–28]. With the inclusion of a spatially absorbing sample, it has been shown that correlated photons can be used to suppress noise in imaging objects to a degree that outperforms classical measurement using an equally efficient detection [8,29]. Since absorption measurement is the most versatile tool for many applications in spectroscopy, metrology, chemistry, and biology, improving the measurement sensitivity is thus indisputably beneficial to both the science and the engineering communities. It is therefore most valuable for experiments to be performed to observe the clear quantum advantages that are gained by using quantum states of light in absorption measurements.

Indeed, quantum advantages in absorption measurements have been demonstrated in a series of experiments carried out with photon pairs generated using SPDC in nonlinear crystals; for some prominent examples, see Refs. [2,9,12,13]. It should be noted that SPDC is not the only source of quantum light; another important quantum source is the squeezed light produced with four-wave mixing (FWM) in atomic vapors or optical fibers [30]. In fact, squeezed light has been extensively studied for its advantage in phase measurement since the early prediction of Caves [31]; some prominent experiments are reported in Refs. [15,19,22,32]. However, there have been hardly any experimental demonstrations using squeezed light to achieve sub-SNL absorption measurements since the seminal work done by Polzik *et al.* [33]. In this paper, we report a practically realizable experimental scheme using squeezed light for direct-absorption measurements. We use intensity-squeezed beams generated with a seeded FWM process as the source to demonstrate clear quantum advantages over the SNL. Note that Moreau *et al.* [13] have reported a quantum advantage of 0.9 dB using SPDC in direct-absorption measurements, while we report a higher quantum advantage of more than 1.2 dB for weak absorption levels ( $\leq 10\%$ ), as shown below.

Our experimental scheme is straightforward—a seeded FWM atomic vapor cell together with an electron-multiplying charge-coupled-device (EMCCD) camera comprise the bulk of what is needed to acquire a sub-SNL absorption measurement. Information containing absorption of the sample being measured can be readily obtained by simply integrating the images captured by the EMCCD camera and no homodyne or lock-in or logic coincidence is required. Our scheme is therefore very applicable in many circumstances where sub-SNL absorption measurement is

highly desirable. We also provide in this paper a theoretical model to analyze and gain insights into the experimental observations.

## II. RESULTS

### A. Theoretical analysis of the quantum advantage for measurement sensitivity

Our intensity-squeezed light is generated with the FWM process in an atomic  $^{85}\text{Rb}$  vapor cell [15,34–38]. The atomic medium possesses a large third-order electric susceptibility  $\chi^{(3)}$  and when appropriately chosen laser light “seeds” the medium, “twin beams,” also known as the “probe” and “conjugate” beams, are produced. The theoretical modeling of the twin-beam generation in the FWM process is complex, as in the experiment one deals with the probe and conjugate beams of finite bandwidth. In fact, the bandwidth of the twin beams in our scheme is merely approximately 20 MHz [38,39], which is much narrower compared to what one generates with SPDCs. Therefore, we can recover many of the aspects of our observations in terms of a theoretical model based on an equivalent *single-mode* description of the probe and conjugate beams [36]. In brief, we use the single-mode approximation and designate  $\hat{a}$  and  $\hat{b}$  as the mode operators for the probe and conjugate beams, respectively. The final operators after detection can therefore be expressed as

$$\begin{aligned}\hat{a}_f &= \sqrt{\eta_p}\{\sqrt{1-\alpha}[(\cosh r)\hat{a} + e^{i\theta}(\sinh r)\hat{b}^\dagger] + i\sqrt{\alpha}\hat{v}_\alpha\} \\ &\quad + i\sqrt{1-\eta_p}\hat{v}_p, \\ \hat{b}_f^\dagger &= \sqrt{\eta_c}[(\cosh r)\hat{b}^\dagger + e^{-i\theta}(\sinh r)\hat{a}] - i\sqrt{1-\eta_c}\hat{v}_c^\dagger,\end{aligned}\quad (1)$$

where  $r$  is the squeezing parameter of the FWM,  $\theta$  is the relative phase between the twin beams [approximately  $\theta \cong 2\pi \times 2\nu_{\text{HF}} \times L/c$ , where  $2\nu_{\text{HF}}$  is the frequency difference between the twin beams,  $\nu_{\text{HF}}$  is the hyperfine splitting in the electronic ground state of  $^{85}\text{Rb}$ , shown in Fig. 1(b),  $L$  is the vapor cell length, and  $c$  is the speed of light],  $1-\eta_p$  and  $1-\eta_c$  are the optical losses including imperfect detection quantum efficiencies in the probe-beam and conjugate-beam paths, respectively,  $\alpha$  is the absorption we are interested in measuring, and  $\hat{v}_p$ ,  $\hat{v}_c$ , and  $\hat{v}_\alpha$  are the vacuum or noise operators. When a coherent state  $|\beta\rangle$ ,  $\beta = |\beta|e^{i\phi}$ , where  $\phi$  is the input phase, seeds mode  $a$  and only vacuum fluctuations  $|0\rangle$  seed mode  $b$ , then the input state can be written as  $|\beta, 0, 0, 0, 0\rangle$ , where the third, fourth, and fifth zeros are the inputs for the vacuum or noise operators  $\hat{v}_p$ ,  $\hat{v}_c$  and  $\hat{v}_\alpha$ , respectively. Although not trivial, it is fairly straightforward to calculate the number operators  $\hat{N}_a = \hat{a}_f^\dagger \hat{a}_f$  and  $\hat{N}_b = \hat{b}_f^\dagger \hat{b}_f$  for the probe and conjugate beams after detection. Since the sample is placed in the probe beam and the conjugate beam is

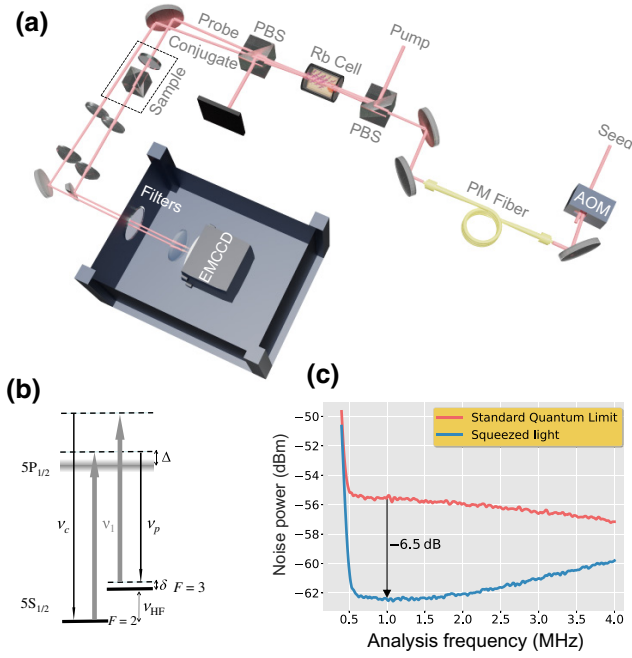


FIG. 1. (a) The experimental setup, in which a seeded  $^{85}\text{Rb}$  vapor cell produces strong quantum-correlated twin beams via FWM. The twin beams are separated from the pump by an approximately  $2 \times 10^5 : 1$  polarizer after the cell. The probe beam passes through an absorption “sample” (i.e., a combination of a  $\lambda/2$  plate and a polarizing beam splitter), while the conjugate beam serves as a reference, before they are focused onto an EMCCD camera. The camera is enclosed in a light-proof box with filters mounted to block ambient light. The AOM in the probe-beam path is used to pulse the twin beams with  $2 \mu\text{s}$  FWHM and a duty cycle of  $1/12$ . PBS, polarizing beam splitter; PM fiber, polarization-maintaining fiber. (b) The level structure of the  $D_1$  transition of the  $^{85}\text{Rb}$  atom. The optical transitions are arranged in a double- $\Lambda$  configuration, where  $\nu_p$ ,  $\nu_c$ , and  $\nu_1$  stand for the probe, conjugate, and pump frequencies, respectively, fulfilling  $\nu_p + \nu_c = 2\nu_1$ . The width of the excited state in the level diagram represents the Doppler-broadened line.  $\Delta$  is the one-photon detuning,  $\delta$  is the two-photon detuning, and  $\nu_{\text{HF}}$  is the hyperfine splitting in the electronic ground state of  $^{85}\text{Rb}$ . (c) The measured intensity-difference noise-power spectrum for the squeezed twin beams (blue line) and for the SNL (red line), obtained with a radio-frequency spectrum analyzer (with a resolution and a video bandwidth of 300 kHz and 100 Hz, respectively). A squeezing of 6.5 dB is achieved.

used as a reference, we adopt the photon-counts difference  $\langle \hat{S}_\alpha \rangle = \langle \hat{N}_a - \hat{N}_b \rangle$  as our measurement signal. Note that this double-beam approach is commonly implemented in imaging and spectroscopy applications involving weak absorption [8,26], because it enables the cancellation of classical super-Poissonian noise and provides a direct measurement of the absorption by instantaneous comparison with the unperturbed reference beam. The measurement

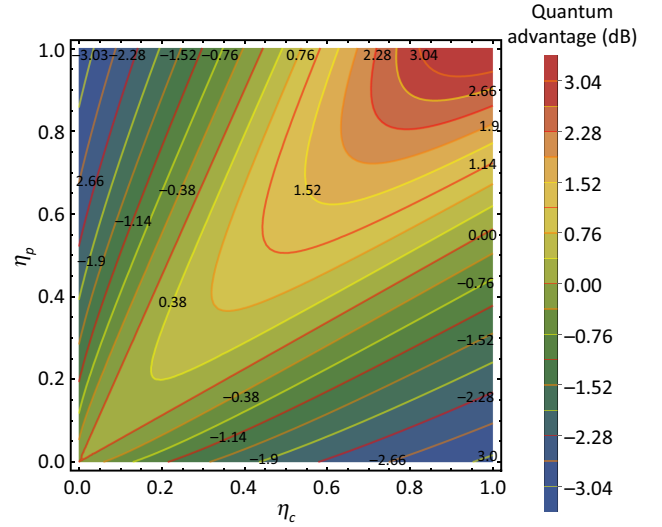


FIG. 2. The theoretical prediction for the quantum advantage (Qu. Adv.) for absorption  $\alpha = 5\%$  as a function of optical transmission in the probe-beam path  $\eta_p$  and the conjugate-beam path  $\eta_c$ . The squeezing parameter  $r = 1.1$  corresponds to 6.5 dB two-mode squeezing.

sensitivity,

$$\Delta\alpha = \frac{\sqrt{\langle \Delta^2 \hat{S}_\alpha \rangle}}{|\partial_\alpha \langle \hat{S}_\alpha \rangle|}, \quad (2)$$

can then be readily obtained. In this paper, we define the quantum advantage as the ratio of the sensitivity enabled by the squeezed light,  $\Delta\alpha_{\text{sqz}}$ , to that acquired from the coherent light,  $\Delta\alpha_{\text{snl}}$ , with the same amount of average photon numbers  $\langle N_a \rangle$  and  $\langle N_b \rangle$  as the twin beams:

$$\text{quantum advantage (dB)} = 10 \times \log_{10} \frac{\Delta\alpha_{\text{sqz}}}{\Delta\alpha_{\text{snl}}}. \quad (3)$$

In Fig. 2, we plot the theoretical quantum advantage for absorption  $\alpha = 5\%$  as a function of optical transmission in the probe-beam path  $\eta_p$  and the conjugate-beam path  $\eta_c$ . The squeezing parameter  $r = 1.1$ , which is calculated from the two-mode squeezing of 6.5 dB [36] measured by near-perfect photodiodes (for further details of the squeezing measurement, see Fig. 1(c) and Ref. [40]). It is clearly noticeable from the graph that if one could manage to curb the optical loss in both beam paths to be within 10%, more than 3 dB quantum advantage for the measurement sensitivity would be readily achievable.

## B. Experimental demonstration of the quantum advantage

The experimental setup and the respective  $^{85}\text{Rb}$  atomic level structure are shown in Figs. 1(a) and 1(b). The

atomic medium is pumped by a strong (approximately 500 mW) narrow-band continuous-wave (cw) laser at frequency  $\nu_1$  ( $\lambda = 795$  nm) with a typical line width  $\Delta\nu_1 \sim 100$  kHz. Applying an additional weak (approximately 10 nW) coherent seed beam at frequency  $\nu_p = \nu_1 - (\nu_{\text{HF}} + \delta)$ , where  $\nu_{\text{HF}}$  and  $\delta$  are the hyperfine splitting in the electronic ground state of  $^{85}\text{Rb}$  and the two-photon detuning, respectively, in Fig. 1(b) (further experimental details can be found in Ref. [40]), two pump photons are converted into a pair of twin photons, namely “probe  $\nu_p$ ” and “conjugate  $\nu_c$ ” photons, adhering to the energy conservation  $2\nu_1 = \nu_p + \nu_c$  [see the level structure in Fig. 1(b)]. The resulting twin beams are strongly quantum correlated and are also referred to as bright two-mode squeezed light [41]. As can be seen from Fig. 1(c), the twin beams exhibit a intensity-difference squeezing of 6.5 dB measured by balanced photodiodes (for further details on the squeezing measurement, see Ref. [40]), which is indicative of strong quantum correlations [41].

After the  $^{85}\text{Rb}$  vapor cell, the pump and the twin beams are separated by a second polarizer, with an approximately  $2 \times 10^5 : 1$  extinction ratio for the pump. The probe beam transverses through a combination of a  $\lambda/2$  plate and a PBS, acting as an absorption sample, while the conjugate beam serves as a reference. The twin beams are then focused onto an EMCCD camera (Andor iXon Ultra 897). The EMCCD camera is enclosed in a light-proof box with filters installed at the entrance to block ambient light photons from entering the camera. The acousto-optic modulator (AOM) in the probe-beam path is used to pulse the beam with  $2 \mu\text{s}$  duration (FWHM) and a duty cycle of

1/12. Since the cw pump beam is present all the time, the conjugate beam is therefore also pulsed as a result of the FWM process. The time sequencing of the pump and the twin beams are shown in Fig. 3(a) as the red strap and the blue and green squares, respectively.

We acquire the temporal behavior of the twin beams through the use of the *kinetic* mode of the EMCCD camera. The EMCCD camera has  $512 \times 512$  pixels with each pixel of size  $16 \mu\text{m} \times 16 \mu\text{m}$ . We focus the twin beams on the camera with an  $1/e^2$  beam diameter of approximately  $50 \mu\text{m}$ , occupying roughly 3 pixels as shown in Fig. 3(b). The temperature of the EMCCD camera is kept low ( $< -65^\circ\text{C}$ ) to curb the thermal noise contributions. The rest of the EMCCD camera settings can be found in Ref. [40].

For each absorption  $\alpha$  (acquired by changing the angle of the  $\lambda/2$  plate), we capture 200 kinetic series, i.e., 200 frame sequences, with each frame having 35 pairs of probe and conjugate images containing the desired absorption information. We then crop a  $10 \times 10$  pixel region around the maximum-intensity area in each probe and conjugate images, large enough to enclose their respective full beam profiles [see Fig. 3(b)]; we thus can obtain the average total number of photons in the probe beam  $\bar{N}_p$  and in the conjugate beam  $\bar{N}_c$  by integrating photon counts in the cropped regions.

The measurement signal  $S_\alpha$  is defined as the photon-number difference between the probe and conjugate beams:

$$S_\alpha \equiv \bar{N}_p - \bar{N}_c = (1 - \alpha)\bar{N}_{p0} - \bar{N}_c, \quad (4)$$

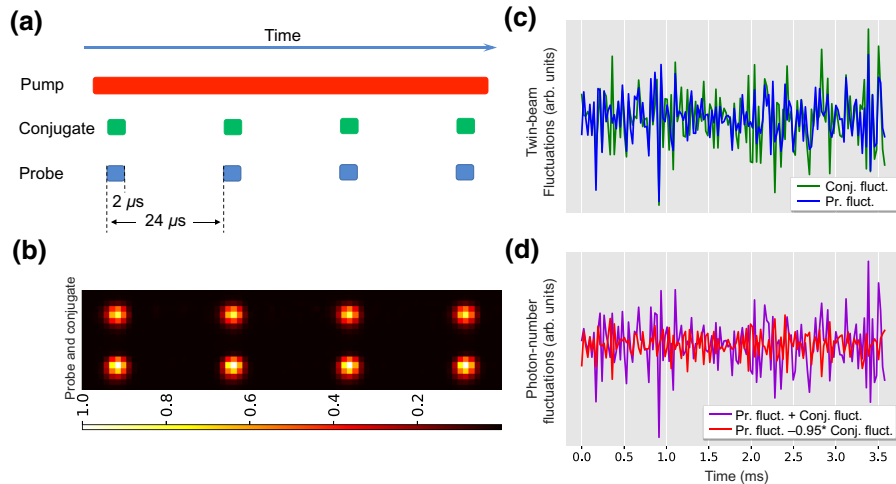


FIG. 3. (a) The time sequencing of the pump and twin beams. The pulse duration of  $2 \mu\text{s}$  and the duty cycle of 1/12 are realized by pulsing the probe beam with an AOM. The cw pump beam is present all the time. (b) Typical images of the twin beams with absorption  $\alpha = 3\%$  captured by the EMCCD camera. This panel is the “real-life” version of panel (a). It is an image of four consecutive pulses with the pulse width and duty cycle shown in panel (a). (c) The temporal photon-count fluctuations of the probe  $N_p(t)$  and the conjugate  $N_c(t)$  obtained by integrating the photon counts in the cropped regions in (b). Clear similarities can be observed between the twin beams. (d) The strong noise reduction in the subtraction as opposed to the summation of the  $N_p(t)$  and  $N_c(t)$  depicted in (c) showcases strong correlations between them.



where  $\bar{N}_{p0}$  and  $\bar{N}_p$  are the average numbers of photons in the probe beam before and after the faint absorber, respectively, and  $\bar{N}_c$  is the average number of photons in the conjugate beam. Factoring out  $\alpha$ , we have

$$\alpha = -\frac{1}{\bar{N}_{p0}}S_\alpha + \frac{S_0}{\bar{N}_{p0}}, \quad (5)$$

where  $S_0 \equiv \bar{N}_{p0} - \bar{N}_c$  is the photon-number difference of the twin beams without the presence of the absorber, which can be treated as a characteristic of the quantum light source itself.

Also, the relation between the uncertainties of absorption  $\alpha$  and the measurement signal  $S_\alpha$  can be derived from the error-propagation formula [see Eq. (2)]:

$$\Delta\alpha = \frac{\Delta S_\alpha}{|\partial_\alpha S_\alpha|} = \frac{1}{\bar{N}_{p0}} \Delta S_\alpha, \quad (6)$$

where  $|\partial_\alpha S_\alpha| = \bar{N}_{p0}$  is obtained from Eq. (4). Therefore, following Eqs. (5) and (6), the absorption  $\alpha$  and its sensitivity  $\Delta\alpha$  can be readily obtained from the measurements of  $S_\alpha$  and  $\Delta S_\alpha$ .

In Fig. 4, we plot the actual absorption  $\alpha$  as a function of the measurement signal  $S_\alpha$ . The inset in Fig. 4 is an enlarged view of the data points with absorption  $\alpha < 10\%$  to illustrate the sizes of uncertainties of these two quantities, i.e.,  $\Delta S_\alpha$  on the x axis and  $\Delta\alpha$  on the y axis. In the experiment, we observe  $1.3 \pm 0.2$  dB quantum advantage in terms of  $\Delta S_\alpha$  when comparing to shot-noise-limited classical measurements for faint absorption levels (see Fig. 6). Due to the fact that  $\Delta\alpha \propto \Delta S_\alpha$ , with  $1/\bar{N}_{p0}$  being the proportionality constant [see Eq. (6)], this greater than 1 dB quantum advantage should also translate to  $\Delta\alpha$  when compared to its shot-noise-limited classical counterparts.

For measurements of the quantum noise reduction between the twin beams, we adopt an algorithm originally developed in the spatial domain [27,28] but rederiving it in the temporal domain. As shown in Fig. 3(c), the temporal photon-count fluctuations of the probe beam  $N_p(t)$  and the conjugate beam  $N_c(t)$  are acquired by integrating photon counts in the cropped  $10 \times 10$  pixel regions for 7000 pairs of twin-beam images during 170 ms. As expected, strong correlations between the photon-count fluctuations of the twin beams can be observed in Fig. 3(c) and manifested in Fig. 3(d) through the subtraction and addition of these two modes. The quantum noise-reduction characterization,  $\sigma$ , in the temporal domain reads

$$\sigma \equiv \frac{\langle \Delta^2[(N_p(t+\delta t) - N_p(t)) - \eta(N_c(t+\delta t) - N_c(t))] \rangle_t}{\langle N_p(t+\delta t) + N_p(t) + \eta N_c(t+\delta t) + \eta N_c(t) \rangle_t}, \quad (7)$$

where  $N_p(t+\delta t) - N_p(t)$  and  $N_c(t+\delta t) - N_c(t)$  are the subtractions of photon counts in the cropped regions in two

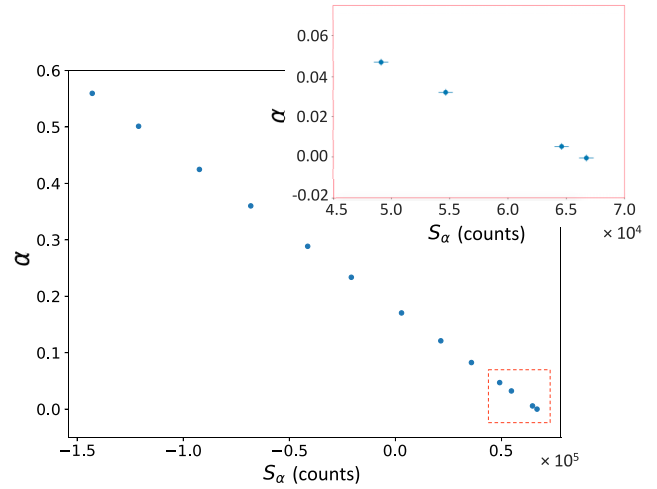


FIG. 4. The actual absorption  $\alpha$  as a function of the measurement signal  $S_\alpha$  defined in Eq. (4). The inset is an enlarged view of the data points with absorption  $\alpha < 10\%$  to illustrate the sizes of the uncertainties on the x axis,  $\Delta S_\alpha$ , and the uncertainties on the y axis,  $\Delta\alpha$ .

successive probe and conjugate images with time interval of  $\delta t = 24 \mu\text{s}$ . Since the intensities of the twin beams are inherently imbalanced due to the seed power and different transmissions through the vapor cell [36], a scaling factor  $\eta = 0.95$ , which is obtained by taking the ratio between the conjugate and probe photon counts in the analysis regions without the presence of the absorption sample, is applied to the conjugate mode to rescale its photon count before the two modes are subtracted. Note that each image is involved in averaging over the spatial intensity profile of the beam and that the scaling factor effectively balances not only any differences in the averaging of the beam intensity profiles but also the intensity fluctuations. The subtraction of two successive images leads to the cancellation of the low-frequency portion of the classical noise so that the rest of fluctuations are in the shot-noise-limited regime [27,28]. The numerator of Eq. (7) represents the temporal variance of the intensity-difference noise between the probe and conjugate pulses. The denominator gives the mean photon counts for the probe and conjugate pulses used for the analysis and represents the shot noise. For coherent state pulses  $\sigma = 1$ , which corresponds to the SNL, while for thermal light or other classical states,  $\sigma > 1$ . Temporally quantum-correlated beams, such as the twin beams generated in our experiment, will result in  $\sigma < 1$ , with a smaller  $\sigma$  corresponding to a larger degree of quantum correlations (i.e., two-mode squeezing).

In Fig. 5, we plot  $\sigma$  as a function of the absorption  $\alpha$  for the squeezed light together with the coherent light. For each  $\alpha$ , we average five sets of 200 kinetic series and designate the error bar with one standard deviation. As expected,  $\sigma < 1$  for the squeezed light (blue squares), while  $\sigma \cong 1$  when the twin beams are replaced with two

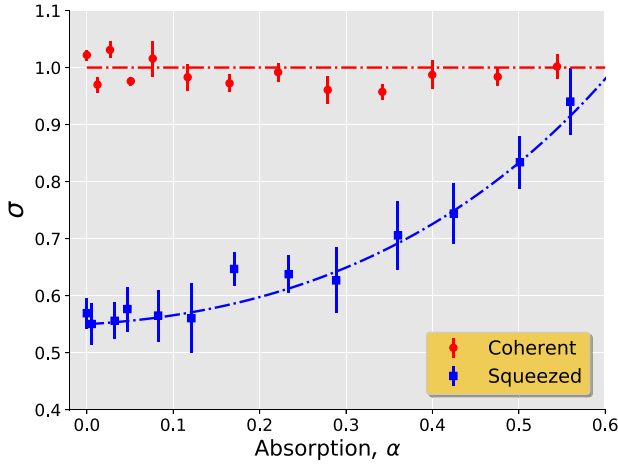


FIG. 5. The temporal quantum noise reduction  $\sigma$  as a function of the absorption  $\alpha$  for the intensity-squeezed light (blue squares) and the coherent light (red dots). The dashed blue line is the theoretical prediction with  $\eta_p = 0.61$ ,  $\eta_c = 0.63$ , and  $r = 1.1$ .

coherent beams (red dots). The notable degradation of the temporal quantum noise reduction measured by the EMCCD camera with respect to that measured by balanced photodiodes in Fig. 1(c) can be mainly attributed to a much worse quantum efficiency of the EMCCD camera at 795 nm (merely 70% as opposed to at least 94% for photodiodes). We also repeat the experiment with different pulse duty cycles [i.e.,  $\delta t$  in Eq. (7)], but they seem to play a nonessential role in the quantum noise reduction as long as we are in the shot-noise-limited regime, i.e.,  $\sigma$  is still close to unity for coherent beams.

From Eqs. (2) and (3), we can easily arrive at

$$\begin{aligned} \text{quantum advantage (dB)} &= 10 \times \log_{10} \frac{\Delta\alpha_{\text{sqz}}}{\Delta\alpha_{\text{snl}}} \\ &= 10 \times \log_{10} \sqrt{\frac{\langle \Delta^2 \hat{N}_\alpha \rangle_{\text{snl}}}{\langle \Delta^2 \hat{N}_\alpha \rangle_{\text{sqz}}}} = 10 \times \log_{10} \sqrt{\frac{1}{\sigma}}. \end{aligned} \quad (8)$$

We can thus use the same data as depicted in Fig. 5 to plot the quantum advantage versus the absorption  $\alpha$ . The results are shown in Fig. 6. Theoretical predictions for the temporal quantum noise-reduction characterization  $\sigma$  and the quantum advantage as a function of the absorption  $\alpha$  are plotted as dashed blue lines in Figs. 5 and 6, where excellent agreement between experiment and theory can be seen. At those faint absorption levels ( $\alpha \leq 10\%$ ) in Fig. 6, the observed quantum advantage can be more than 1.2 dB, although the *total* optical losses (including the transmission loss imposed by optics and the imperfect detection quantum efficiency imposed by the EMCCD camera) in the paths of the twin beams are significant—nearly 39% in the probe path and nearly 37% in the conjugate path. This is mainly due to a relatively low quantum efficiency of the EMCCD camera at 795 nm (approximately 70%) and

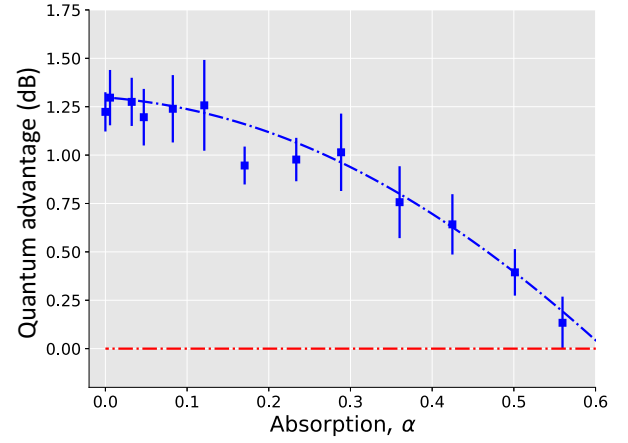


FIG. 6. The quantum advantage as a function of the absorption  $\alpha$ . The dashed blue line is the theoretical prediction with  $\eta_p = 0.61$ ,  $\eta_c = 0.63$ , and  $r = 1.1$ . The quantum advantage is only significant ( $> 1$  dB) for small values of  $\alpha$  ( $< 20\%$ ) and for  $\alpha > 60\%$  there is no quantum advantage.

imperfect transmission of the band-pass filters (approximately 94%) mounted in front of the light-proof box. If we were able to overcome this main obstacle of the experiment by employing a much more efficient camera, we would have a much higher quantum advantage approaching 3 dB, as implied by the theoretical curves in Fig. 2. We note that a very recent work [14] has also demonstrated quantum advantage in absorption measurements using a single-mode amplitude squeezed light generated with an optical phase-sensitive amplifier. The reported advantage (according to Fig. 5 in Ref. [14]) is less than 0.5 dB.

It is worth mentioning that taking measurements using photodetectors would yield better results due to the much higher quantum efficiency of photodiodes. However, the main drawback of using photodetectors is their much higher power requirement. For an EMCCD camera, an input power of a few nanowatts is more than enough to yield a clear signal-to-noise ratio; however, for a photodetector to provide sufficient signal clearance from its electronic noise floor, the input power has to be in the range of tens of microwatts. For example, in our experiment, in order to have a signal noise power that is 10 dB above the electronic noise floor, we have to shine a coherent beam of light of at least  $50 \mu\text{W}$  to the photodetector (given our squeezing level of 6.5 dB, that implies a merely 3.5-dB clearance from the electronic noise floor for  $50 \mu\text{W}$  squeezed light). One of the most important implementations of our experimental scheme is to characterize biological samples without imposing light-induced damage and hence a much higher input light power would defeat this purpose.

### III. DISCUSSION

Overall, our experiment realizes a practical scheme that allows the SNL in the direct-absorption measurement to

be overcome. We demonstrate that by using intensity-squeezed light, a quantum advantage of more than 1.2 dB is achieved for the measurement sensitivity at faint absorption levels ( $\leq 10\%$ ). We thus experimentally demonstrate the advantage of squeezed light for measurements on open systems. We also theoretically demonstrate that more quantum advantage ( $> 3$  dB) is very likely attainable by means of proper optical loss management. We use a seeded FWM process in an atomic  $^{85}\text{Rb}$  vapor cell to generate the quantum-correlated twin beams of light. We use quantum light generated with FWM instead of SPDC to demonstrate a sub-shot-noise absorption measurement. The major advantages of this FWM-based quantum light generation scheme include an ultrahigh photon-pair flux up to  $10^{16}$  photons/s, which is a few orders of magnitude higher than the fluxes produced by SPDCs [42–44] and by narrow-band probe and conjugate beams (approximately 20 MHz) [38,39], which can be readily integrated into quantum networks through coupling with microresonators or cavities. Also, although the small bandwidth feature of the twin beams is not used in the experiment, we do take advantage of it by making a “single-mode” approximation for the twin beams in the theoretical analysis. The fact that our experimental results agree very well with the theory based on the “single-mode” approximation confirms the significance of the narrow-band feature of the twin beams. Moreover, the seeded FWM process offers sufficient gains in a single-pass configuration, producing bright quantum-correlated beams of light without a cavity, making it possible to preserve the multi-spatial-mode nature of the bright twin beams [45,46]. Our quantum light generation, together with the direct-absorption-measurement scheme reported here, can therefore be beneficial to many applications involving the characterization of chemical and biological samples, where sub-SNL absorption measurements are highly desirable [47,48].

### ACKNOWLEDGMENTS

We gratefully acknowledge the support of the Air Force Office of Scientific Research (Award No. FA-9550-18-1-0141), the Office of Naval Research (Award No. N00014-20-1-2184), and the Robert A. Welch Foundation (Grants No. A-1261 and No. A-1943). F.L. acknowledges support from the Herman F. Heep and Minnie Belle Heep Texas A&M University Endowed Fund administered by the Texas A&M Foundation.

- 
- [1] P. R. Tapster, S. F. Seward, and J. G. Rarity, Sub-shot-noise measurement of modulated absorption using parametric down-conversion, *Phys. Rev. A* **44**, 3266 (1991).  
 [2] P. H. S. Ribeiro, C. Schwob, A. Maître, and C. Fabre, Sub-shot-noise high-sensitivity spectroscopy with optical parametric oscillator twin beams, *Opt. Lett.* **22**, 1893 (1997).

- [3] M. M. Hayat, A. Joobeur, and B. E. A. Saleh, Reduction of quantum noise in transmittance estimation using photon-correlated beams, *J. Opt. Soc. Am. A* **16**, 348 (1999).  
 [4] N. Treps, N. Grosse, W. P. Bowen, C. Fabre, H.-A. Bachor, and P. K. Lam, A quantum laser pointer, *Science* **301**, 940 (2003).  
 [5] V. Giovannetti, S. Lloyd, and L. Maccone, Quantum-enhanced measurements: Beating the standard quantum limit, *Science* **306**, 1330 (2004).  
 [6] E. Brambilla, L. Caspani, O. Jedrkiewicz, L. A. Lugiato, and A. Gatti, High-sensitivity imaging with multi-mode twin beams, *Phys. Rev. A* **77**, 053807 (2008).  
 [7] W. N. Plick, P. M. Anisimov, J. P. Dowling, H. Lee, and G. S. Agarwal, Parity detection in quantum optical metrology without number-resolving detectors, *New J. Phys.* **12**, 113025 (2010).  
 [8] G. Brida, M. Genovese, and I. Ruo Berchera, Experimental realization of sub-shot-noise quantum imaging, *Nat. Photonics* **4**, 227 (2010).  
 [9] F. Wolfgramm, C. Vitelli, F. A. Beduini, N. Godbout, and M. W. Mitchell, Entanglement-enhanced probing of a delicate material system, *Nat. Photonics* **7**, 28 (2013).  
 [10] M. A. Taylor, J. Janousek, V. Daria, J. Knittel, B. Hage, H.-A. Bachor, and W. P. Bowen, Biological measurement beyond the quantum limit, *Nat. Photonics* **7**, 229 (2013).  
 [11] M. A. Taylor and W. P. Bowen, Quantum metrology and its application in biology, *Phys. Rep.* **615**, 1 (2016).  
 [12] R. Whittaker, C. Erven, A. Neville, M. Berry, J. L. O’Brien, H. Cable, and J. C. F. Matthews, Absorption spectroscopy at the ultimate quantum limit from single-photon states, *New J. Phys.* **19**, 023013 (2017).  
 [13] P.-A. Moreau, J. Sabines-Chesterking, R. Whittaker, S. K. Joshi, P. M. Birchall, A. McMillan, J. G. Rarity, and J. C. F. Matthews, Demonstrating an absolute quantum advantage in direct absorption measurement, *Sci. Rep.* **7**, 6256 (2017).  
 [14] G. Triginer Garces, H. M. Chrzanowski, S. Daryanoosh, V. Thiel, A. L. Marchant, R. B. Patel, P. C. Humphreys, A. Datta, and I. A. Walmsley, Quantum-enhanced stimulated emission detection for label-free microscopy, *Appl. Phys. Lett.* **117**, 024002 (2020).  
 [15] B. E. Anderson, P. Gupta, B. L. Schmittberger, T. Horrom, C. Hermann-Avigliano, K. M. Jones, and P. D. Lett, Phase sensing beyond the standard quantum limit with a variation on the SU(1,1) interferometer, *Optica* **4**, 752 (2017).  
 [16] W. N. Plick, J. P. Dowling, and G. S. Agarwal, Coherent-light-boosted, sub-shot noise, quantum interferometry, *New J. Phys.* **12**, 083014 (2010).  
 [17] A. Kolkiran and G. S. Agarwal, Quantum interferometry using coherent beam stimulated parametric down-conversion, *Opt. Express* **16**, 6479 (2008).  
 [18] N. Thomas-Peter, B. J. Smith, A. Datta, L. Zhang, U. Dorner, and I. A. Walmsley, Real-World Quantum Sensors: Evaluating Resources for Precision Measurement, *Phys. Rev. Lett.* **107**, 113603 (2011).  
 [19] The LIGO Scientific Collaboration, A gravitational wave observatory operating beyond the quantum shot-noise limit, *Nat. Physics* **7**, 962 (2011).  
 [20] S. N. Arhipov, I. Saytashev, and M. Dantus, Intravital imaging study on photodamage produced by femtosecond near-infrared laser pulses *in vivo*, *Photochem. Photobiol.* **92**, 308 (2016).

- [21] G. Y. Xiang, B. L. Higgins, D. W. Berry, H. M. Wiseman, and G. J. Pryde, Entanglement-enhanced measurement of a completely unknown optical phase, *Nat. Photonics* **5**, 43 (2011).
- [22] H. Yonezawa, D. Nakane, T. A. Wheatley, K. Iwasawa, S. Takeda, H. Arao, K. Ohki, K. Tsumura, D. W. Berry, T. C. Ralph, H. M. Wiseman, E. H. Huntington, and A. Furusawa, Quantum-enhanced optical-phase tracking, *Science* **337**, 1514 (2012).
- [23] A. A. Berni, T. Gehring, B. M. Nielsen, V. Händchen, M. G. A. Paris, and U. L. Andersen, *Ab initio* quantum-enhanced optical phase estimation using real-time feedback control, *Nat. Photonics* **9**, 577 (2015).
- [24] T. S. Iskhakov, V. C. Usenko, U. L. Andersen, R. Filip, M. V. Chekhova, and G. Leuchs, Heralded source of bright multi-mode mesoscopic sub-Poissonian light, *Opt. Lett.* **41**, 2149 (2016).
- [25] T. Ono, R. Okamoto, and S. Takeuchi, An entanglement-enhanced microscope, *Nat. Commun.* **4**, 2426 (2013).
- [26] N. Samantaray, I. Ruo-Berchera, A. Meda, and M. Genovese, Realization of the first sub-shot-noise wide field microscope, *Light: Sci. Appl.* **6**, e17005 (2017).
- [27] A. Kumar, H. Nunley, and A. M. Marino, Observation of spatial quantum correlations in the macroscopic regime, *Phys. Rev. A* **95**, 053849 (2017).
- [28] A. Kumar and A. M. Marino, Spatial squeezing in bright twin beams generated with four-wave mixing: Constraints on characterization with an electron-multiplying charge-coupled-device camera, *Phys. Rev. A* **100**, 063828 (2019).
- [29] E. Knyazev, F. Y. Khalili, and M. V. Chekhova, Overcoming inefficient detection in sub-shot-noise absorption measurement and imaging, *Opt. Express* **27**, 7868 (2019).
- [30] B. J. Lawrie, P. D. Lett, A. M. Marino, and R. C. Pooser, Quantum sensing with squeezed light, *ACS Photonics* **6**, 1307 (2019).
- [31] C. M. Caves, Quantum-mechanical noise in an interferometer, *Phys. Rev. D* **23**, 1693 (1981).
- [32] P. Gupta, B. L. Schmittberger, B. E. Anderson, K. M. Jones, and P. D. Lett, Optimized phase sensing in a truncated SU(1,1) interferometer, *Opt. Express* **26**, 391 (2018).
- [33] E. S. Polzik, J. Carri, and H. J. Kimble, Spectroscopy with Squeezed Light, *Phys. Rev. Lett.* **68**, 3020 (1992).
- [34] M. Dowran, A. Kumar, B. J. Lawrie, R. C. Pooser, and A. M. Marino, Quantum-enhanced plasmonic sensing, *Optica* **5**, 628 (2018).
- [35] L. Cao, J. Qi, J. Du, and J. Jing, Experimental generation of quadruple quantum-correlated beams from hot rubidium vapor by cascaded four-wave mixing using spatial multiplexing, *Phys. Rev. A* **95**, 023803 (2017).
- [36] T. Li, B. E. Anderson, T. Horrom, B. L. Schmittberger, K. M. Jones, and P. D. Lett, Improved measurement of two-mode quantum correlations using a phase-sensitive amplifier, *Opt. Express* **25**, 21301 (2017).
- [37] R. C. Pooser and B. Lawrie, Ultrasensitive measurement of microcantilever displacement below the shot-noise limit, *Optica* **2**, 393 (2015).
- [38] J. B. Clark, R. T. Glasser, Q. Glorieux, U. Vogl, T. Li, K. M. Jones, and P. D. Lett, Quantum mutual information of an entangled state propagating through a fast-light medium, *Nat. Photonics* **8**, 515 EP (2014).
- [39] R. T. Glasser, U. Vogl, and P. D. Lett, Stimulated Generation of Superluminal Light Pulses via Four-Wave Mixing, *Phys. Rev. Lett.* **108**, 173902 (2012).
- [40] F. Li, T. Li, and G. S. Agarwal, Temporal quantum noise reduction acquired by an electron-multiplying charge-coupled-device camera, *Opt. Express* **28**, 37538 (2020).
- [41] C. F. McCormick, A. M. Marino, V. Boyer, and P. D. Lett, Strong low-frequency quantum correlations from a four-wave-mixing amplifier, *Phys. Rev. A* **78**, 043816 (2008).
- [42] A. Jechow, A. Heuer, and R. Menzel, High brightness, tunable biphoton source at 976 nm for quantum spectroscopy, *Opt. Express* **16**, 13439 (2008).
- [43] J. P. Villabona-Monsalve, O. Varnavski, B. A. Palfey, and T. Goodson, Two-photon excitation of flavins and flavoproteins with classical and quantum light, *J. Am. Chem. Soc.* **140**, 14562 (2018).
- [44] O. Varnavski, B. Pinsky, and T. Goodson, Entangled photon excited fluorescence in organic materials: An ultrafast coincidence detector, *J. Phys. Chem. Lett.* **8**, 388 (2017).
- [45] N. V. Corzo, A. M. Marino, K. M. Jones, and P. D. Lett, Noiseless Optical Amplifier Operating on Hundreds of Spatial Modes, *Phys. Rev. Lett.* **109**, 043602 (2012).
- [46] N. Corzo, A. M. Marino, K. M. Jones, and P. D. Lett, Multi-spatial-mode single-beam quadrature squeezed states of light from four-wave mixing in hot rubidium vapor, *Opt. Express* **19**, 21358 (2011).
- [47] M. Genovese, Real applications of quantum imaging, *J. Opt.* **18**, 073002 (2016).
- [48] M. I. Kolobov, *Quantum Imaging* (Springer, New York, 2007).